Optica Applicata, Vol. LV, No. 4, 2025
DOI: 10.37190/oa/211819

Study on the hollow extinction ratio of Gaussian vortex light

Cunxia LI[1], Didi FU[1], Yanghe LIU[2], Jian ZHOU[1], Ningju HUI[1], Yanlong WANG[1], Yishan ZHANG[1], Yuanhe TANG[1,*]

[1] School of Science, Xi'an University of Technology, Shaanxi Xi'an 710048, China

[2] School of Mechanical and Precision Instrument Engineering, Xi'an University of Technology, Shaanxi Xi'an 710048, China

[*]Corresponding author: ltp1801@163.com

Optical vortices are beams with spiral phase wave fronts capable of carrying different topological charges. This paper presents the expression for Gaussian vortex light and simulates vortices with topological charges of 0, 1, and 2, revealing a "hollow" extinction phenomenon. We derive the relationship between the radius of Gaussian vortex beams and their topological charges, express the extinction ratio of hollow vortices, and calculate the beam radius. The study demonstrates a linear relationship between the extinction ratio and topological charge (from 1 to 20). The fitting accuracy between the simulated hollow radius and the Gaussian vortex approximated radius reaches 85.93%, with an error margin of 17%. In laboratory experiments using a liquid crystal spatial light modulator, we constructed a vortex light system employing a 532.0 nm laser to generate 10 interference fringes of hollow vortex light with topological charges ranging from 10 to 100 on a CCD detector. Pixel measurements were taken for both inner and outer radii corresponding to these charge patterns, enabling precise calculation of extinction ratio. The experimental results show a similar trend to the theoretical predictions, demonstrating that hollow vortex light with extinction properties holds potential applications in signal encryption.

Keywords: Gaussian line type, vortex light, hollow extinction ratio.

1. Introduction

Vortex light has emerged as a research hotspot both domestically and internationally in recent years. Its phase wavefront structure contains a helical phase factor $\exp(il\theta)$ (where θ is the azimuth angle and l is the topological charge), resulting in a spiral-shaped phase distribution along the propagation axis. This characteristic makes vortex beams commonly referred to as spiral beams. The most distinctive feature of vortex beams is their zero-intensity profile along the propagation axis, giving them a hollow appearance. Vortex light holds broad application prospects in fields such as optical communication [1], particle manipulation [2], optical imaging [3], and information encryption [4]. Current generation methods include geometric mode conversion [5], helical phase plate techniques [6], computational holography [7], programmable liquid crystal spa-

tial light modulator-based approaches [8], and metamaterial surface methods [9]. Since COULLET *et al*. first introduced the concept of "optical vortices" in 1989, research on generating optical vortices using liquid crystal spatial light modulators (LCoS) has seen rapid development [10]. LCoS devices offer advantages like high sensitivity, fast response, and precise control. By generating vortex phase holograms through computer algorithms and loading them onto LCoS, vortex beams with different topological charges can be produced. In 2002, CURTIS *et al*. proposed using reflective pure-phase LCoS to generate vortex beams [11]. In 2012, BO *et al*. developed reflective LCoS-based spatial light modulators capable of generating vortex beams with varying topological charges [12]. In 2024, ZHANG *et al*. extended the vortex light technology from LCoS to communication applications [13]. In 2024, our research team conducted studies on Gaussian vortex beam imaging interferometry based on LCoS technology [14]. This paper quantitatively investigates the central darkening and its proportion in vortex light: First, we theoretically analyzed the mathematical characteristics of Gaussian vortex beams and simulated the intensity and phase of these beams with topological numbers $l = 0$, 1, and 2. Second, we derived equations relating the radius of Gaussian vortex beams to their topological numbers, expressions for the hollow extinction ratio in Gaussian vortex beams, and formulas for beam radii. Finally, we have established an optical system based on LCoS in the laboratory to modulate Gaussian light, using experimental results to calculate hollow extinction ratio of Gaussian vortex beams under different topological numbers.

2. Simulation of vortex light modulation of Gaussian spectral lines

Due to the non-uniform broadening of the spectral line caused by the relative motion velocity between the luminous particle and the detector, the spectral line function caused by the Doppler effect presents a Gaussian line type with the relationship between the luminous frequency [15]:

$$g_{\mathrm{D}}(\nu, \nu_0) = \sqrt{\frac{\ln 2}{\pi}} \frac{1}{\alpha_{\mathrm{D}}} \exp\left[-\frac{\ln 2}{\alpha_{\mathrm{D}}^2}(\nu - \nu_0)^2\right] \tag{1}$$

The center frequency is ν_0, the half height width is

$$\alpha_{\mathrm{D}} = \frac{\nu_0}{c}\sqrt{\frac{2kT}{m}\ln 2} \tag{2}$$

and m and T are the mass of the luminous particle and the ambient temperature, respectively, k and c are the Boltzmann constant and the speed of light in vacuum, respectively, and the maximum value of the Gaussian function is

$$g_{\mathrm{D,\,max}} = g_{\mathrm{D}}(\nu_0, \nu_0) = \sqrt{\frac{\ln 2}{\pi}} \frac{1}{\alpha_{\mathrm{D}}} \tag{3}$$

There are various methods to generate vortex light. The method utilizing reflective liquid crystal LCoS for vortex light generation offers high flexibility and ease of operation, as it only pre-loading holograms on the LCoS to modulate the phase of incident light [16]:

$$\varphi = l\theta - 2\pi \operatorname{int}\left(\frac{l\theta}{2\pi}\right) \tag{4}$$

After the plane wave is modulated by the LCoS phase, the light field at the rear focal plane of the lens becomes [16]:

$$\psi_l(r, \theta, 0) = \pi A^2 J_l(x) \exp(il\theta) \sum_{n=0}^{\infty} \frac{(-1)^{n+l/2} \xi^{l+2n}}{(l/2+n+1)n!(n+l)!} \tag{5}$$

where A is the radius of the system's incident pupil and $J_l(x)$ is a first-order Bezier function of l.

The common expression of the complex amplitude of a Laguerre–Gauss (LG) vortex beam is [17]:

$$E(r, \theta, z) = \frac{c_{lp}^{LG}}{w(z)} \left(\frac{\sqrt{2}\, r}{w(z)}\right)^{|l|} \exp\left(-\frac{r^2}{w^2(z)}\right) L_p^{|l|} \frac{2r^2}{w^2(z)} \exp\left(-ik\frac{r^2}{2R(z)}\right)$$

$$\times \exp(-il\theta) \exp(-ikz) \exp(-i\psi(z)) \tag{6}$$

The Laguerre polynomial is $L_p^{|l|}$ and $c_{lp}^{LG} = \sqrt{2p!/\pi(p+|l|)!}$. When the beam waist radius is set to ω_0, $z_R = \pi w_0^2/\lambda$, other parameters are defined as:

$$w(z) = w_0\sqrt{1+(z/z_R)^2} \tag{7}$$

$$R(z) = z\left[1+(z_R/z)^2\right] \tag{8}$$

$$\psi(z) = (|l|+2p+1)\arctan(z/z_R) \tag{9}$$

Here, p and l represent radial and angular coefficients, respectively, indicating different modes of LG beams. By combining various combinations of p and l values, all forms of vortex light can be generated. The fundamental mode ($p = 0$) of LG beams has its complex amplitude expressed as:

$$E(r, \theta, z) = \frac{c_{l0}}{w(z)} \left(\frac{\sqrt{2}\, r}{w(z)}\right)^{|l|} \exp\left(-\frac{r^2}{w^2(z)}\right)$$

$$\times \exp\left[2ik\frac{r^2}{4(z^2+z_R^2)} - \arctan(z/z_R)\right] \exp(-il\theta) \tag{10}$$

As shown by the vortex factor $\exp(il\theta)$ in Eq. (5) and the $\exp(-il\theta)$ term in Eq. (10), since the topological charge l can take positive, negative integers, or fractions, Eqs. (5) and (10) are essentially equivalent, differing only in representing left-handed *versus* right-handed vortex light. Combining this with Eq. (1), we derived the Gaussian vortex spectral line expression as:

$$E(v, v_0) = E_0 \frac{2}{\alpha_D} \sqrt{\frac{\ln 2}{\pi}} \exp\left[-4\ln 2 \frac{(v - v_0)^2}{\alpha_D^2}\right] \exp(-il\theta) \tag{11}$$

Here E_0 is the maximum amplitude.

Based on the mathematical characteristics of Eq. (11), we modulate Gaussian spectral lines using a simulated light source with a wavelength of 867.7 nm and zero-order LG vortex beams, MATLAB programming was employed to simulate the light intensity and phase of general Gaussian light fields ($l = 0$). The simulation results are shown

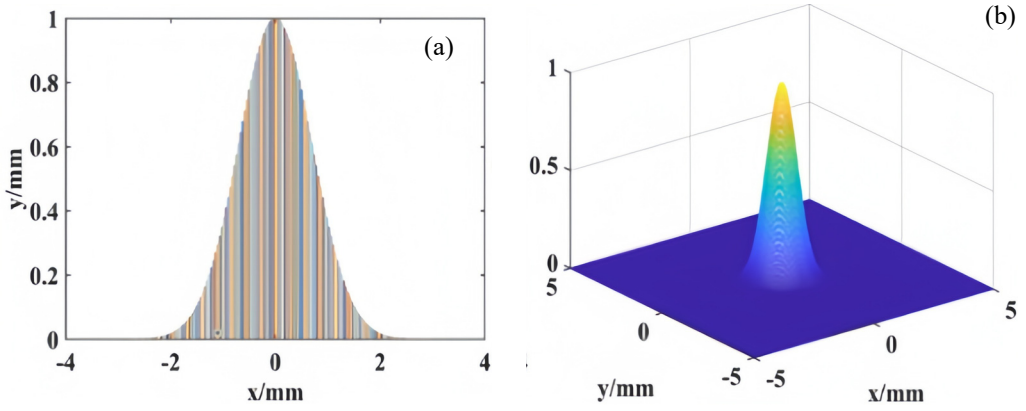

Fig. 1. Simulation diagram of general Gaussian spectral lines without vortex light.

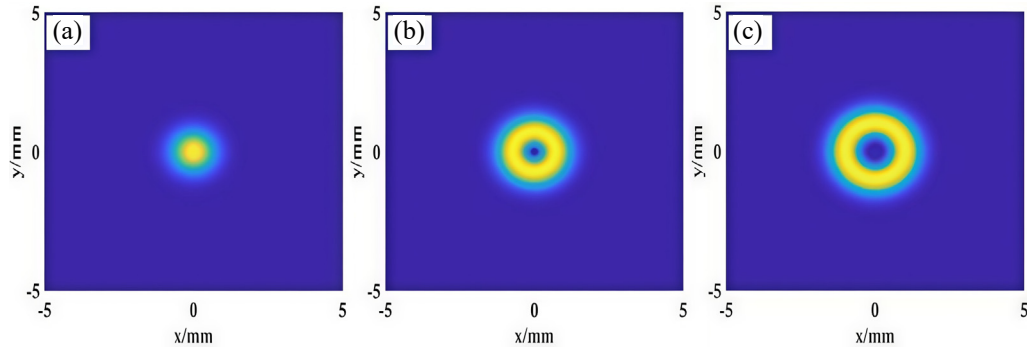

Fig. 2. 2D light intensity of Gaussian vortex optical field with topological number $l = 0$, 1 and 2.

in Fig. 1. By adding a vortex factor, the simulated results of Gaussian vortex lights are presented in Figs. 2–4.

1) Figure 2 shows the 2D light intensity of a Gaussian vortex beam. As the topological charge increases, the intensity pattern gradually transforms into a "donut" shape. The central region of the intensity map exhibits darkening effects that intensify with increasing l values, demonstrating the extinction characteristics of vortex light.

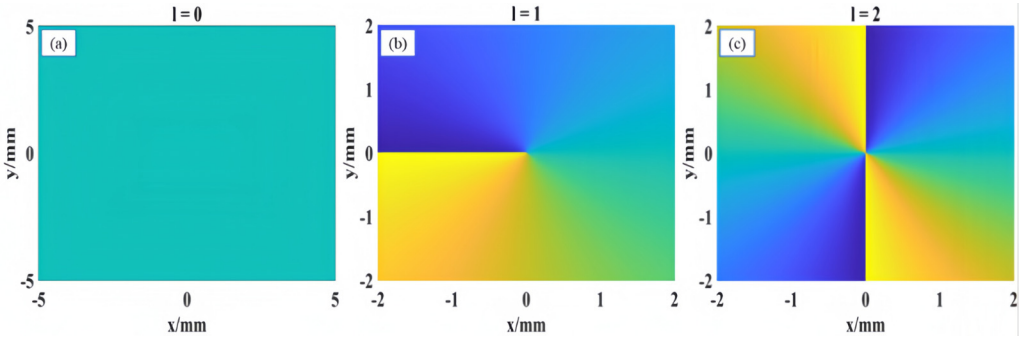

Fig. 3. 2D phase diagram of Gaussian vortex light with topological number l = 0, 1 and 2.

2) Figure 4 shows the 3D light intensity distribution of a Gaussian vortex light beam. At l = 0, the typical Gaussian beam "peaks" remain intact. As l increases, the downward indentation grows progressively, forming a spiral pattern when viewed from above as shown in Fig. 2. Referring to the phase diagram in Fig. 3, it becomes evident that during propagation, the vortex beam undergoes a phase shift of $2\pi l$ per full axial rotation. The overall phase plane exhibits a spiral configuration, where larger l values generate more spiral phases and correspondingly greater phase shifts.

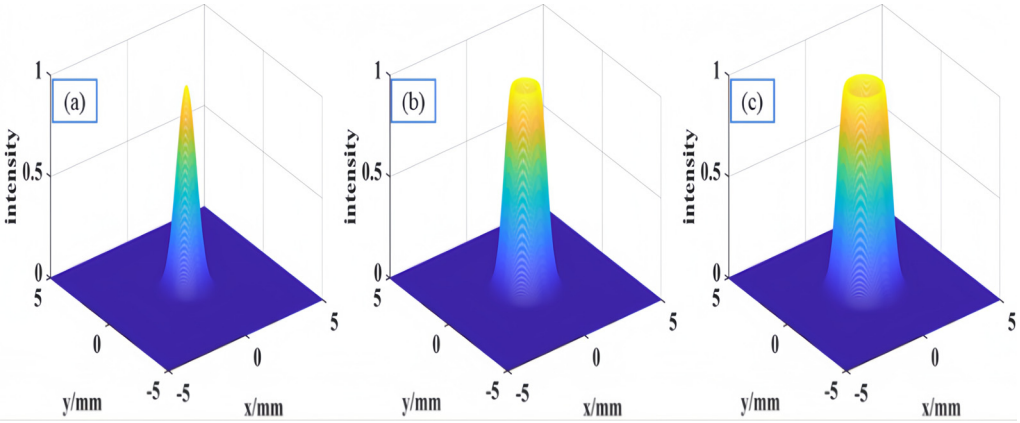

Fig. 4. 3D light intensity map of Gaussian vortex light field with topological number l = 0, 1 and 2.

3. Hollow extinction ratio of high Gaussian vortex light

3.1. Relationship between radius and topological number of Gaussian vortex beam

As shown in Fig. 4, the light intensity image of the Gaussian vortex light has a regular circular "hollow spot" with a certain thickness. The radius of the Gaussian vortex light spot is approximately expressed as follows according to literature [16]:

$$R = \sqrt{|l| + 2p + 0.5}\ \omega_z \tag{12}$$

Here, l is the topological charge, p is the radial coefficient, $\omega_z = w_0\sqrt{1 + z/z_R}$ is the radius of the beam at propagation distance z, and R is the radius length of the outermost layer of the light spot. The LG mode of the low-order fundamental mode ($p = 0$) can be simplified as shown in Eq. (12):

$$R = \sqrt{|l| + 0.5}\ \omega_z \tag{13}$$

Figure 5 illustrates the variation relationship between the radius of the vortex beam at the source plane ($z = 0$) and its topological charge. Theoretically, given the topological charge and beam waist, we can derive a matching relationship from the vortex light as shown in Fig. 5. To verify Eq. (12), we conducted multiple simulations using light

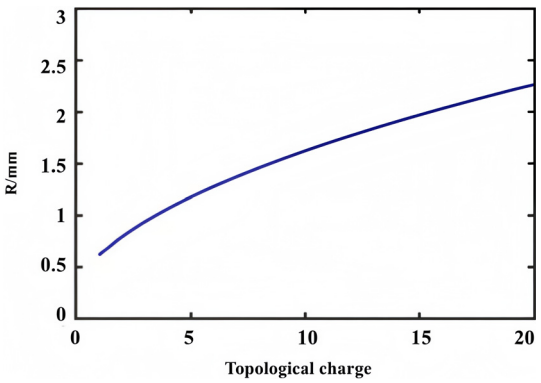

Fig. 5. Linear relationship between R and l at $z = 0$ in Eq. (12).

T a b l e 1. Simulation data of radius of Gaussian vortex beam with topological number l = 1 to 20.

l	R [mm]	l	R [mm]	l	R [mm]	l	R [mm]
1	0.78	6	1.46	11	1.86	16	2.19
2	0.97	7	1.55	12	1.93	17	2.24
3	1.22	8	1.63	13	2.00	18	2.30
4	1.25	9	1.70	14	2.07	19	2.36
5	1.35	10	1.78	15	2.12	20	2.41

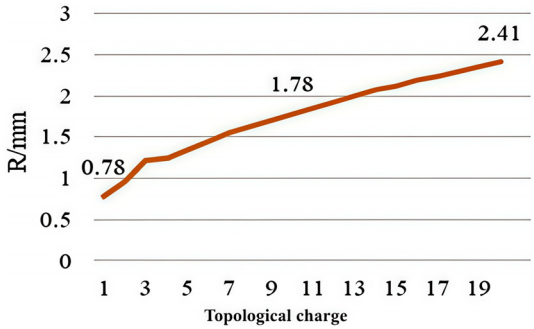

Fig. 6. Simulation results between the vortex beam radius R and l at $z = 0$.

with a wavelength of 867.7 nm. The actual radius R of the vortex beam as a function of l (l = 1 to 20) obtained through MATLAB simulation is presented in Table 1, and the plotted graph of R *versus* l in Fig. 6 demonstrates that the "hollow" radius R of the vortex beam exhibits a linear relationship with l.

By comparing the simulation data in Fig. 6 with the experimental results from Fig. 5 derived from Eq. (12), we observe that the Gaussian vortex beam radius error ranges from l = 1 to 20, approximately 17%. This discrepancy originates from two sources: measurement inaccuracies in the simulation process and inherent errors in our approximate model, which lack precise theoretical formulas for radius calculation. Computational truncation errors and rounding errors are unavoidable during numerical processing. To evaluate the accuracy of Eq. (12) for approximating Gaussian vortex beam radius *versus* Eq. (13) derived from the actual model, repeated simulations showed a 85.93% correlation between the simulated curve in Fig. 6 and the calculated curve in Fig. 5. These results confirm that Eq. (13) can effectively predict the radius of vortex Gaussian beams.

3.2. Limit topological charge of vortex beam

From Eq. (13), we can see that the variation rate of Gaussian vortex light radius R with topological charge l is:

$$\left(\frac{\mathrm{d}R}{\mathrm{d}l}\right)_{z=0} = \frac{w_0}{2\sqrt{l+0.5}} \tag{14}$$

Among them w_0 is the radius of the beam. Although there is no zero solution in the above equation, the result tends to zero when l changes to a certain extent. That is, after a certain value of l, the radius of the Gaussian vortex beam will remain basically consistent, and the radius variation curve of the approximate formula is shown in Fig. 7.

As shown in Fig. 7, to obtain the final attenuation value, we derive the horizontal and vertical asymptotes of Eq. (14). Once the fundamental beam is determined, the numerator of Eq. (14) becomes a constant while the denominator continuously increases

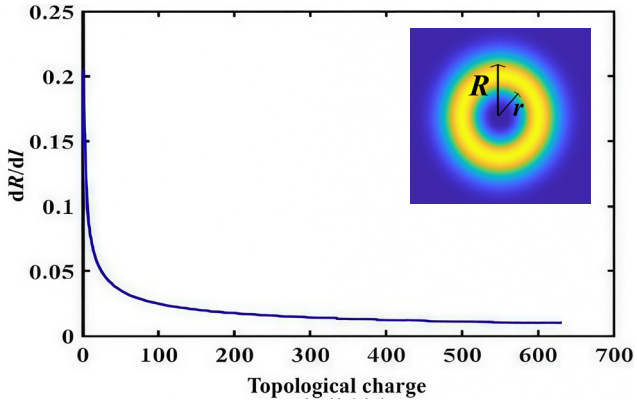

Fig. 7. Change rate curve between Gaussian vortex beam radius R and l, illustration shows a schematic diagram of Gaussian vortex beam radius.

with the topological charge value, eventually approaching zero. Therefore, the horizontal asymptote in Fig. 7 represents the transverse axis itself. For the vertical asymptote, setting l to zero yields:

$$\frac{\mathrm{d}R}{\mathrm{d}l} = \frac{w_0}{\sqrt{2}} \tag{15}$$

When $l = 0$, there exists a fixed length value, such as the vertical asymptote line in Fig. 7, which is half of the size of the pure Gaussian beam spot. The coefficient $1/\sqrt{2}$ is generated when taking approximations. When $l = 0$, only this coefficient needs to be removed to know the waist radius of the base beam.

3.3. Limiting topological charge in extinction vortex beam

For the Gaussian vortex beam, we give the definition of extinction ratio: the ratio of the total area of non-luminous center at a certain position to the total area of circular region formed by the outer radius of bright ring under a certain topological charge l:

$$\Lambda = \frac{S_\mathrm{r}}{S_\mathrm{R}} \times 100\% \tag{16}$$

Here, S_r and S_R correspond to the areas enclosed by the inner and outer rings of vortex light generated by a specific topological charge l. Since experimental measurements require determining the ring's radius while considering its relatively small total area, the topological charge l range for the vortex beam must be defined under experimental precision requirements. Based on experimental specifications, an identification line length $l_\mathrm{lim} = 0.1$ mm is assumed—specifically. The difference between the radii of the

(l + 1)-th and l-th orders serves as the recognizable line length $R_{l+1} - R_l = 0.1$ mm. Consequently, Eq. (13) yields:

$$R_{l+1} - R_l = \left(\sqrt{l + \frac{3}{2}} + \sqrt{l + \frac{1}{2}}\right) w_0 \tag{17}$$

Let $M = (R_{l+1} - R_l)/w_0$, then

$$l_{\text{lim}} = \frac{1}{M^2}\left[\left(\frac{M^2}{2} - 1\right)^2 - \frac{3}{4}\right] \tag{18}$$

This represents the specific expression for the topological charge l_{lim} of recognizable vortex beams defined by experimental linear requirements. Substituting these linear requirements yields $l_{\text{lim}} = 5$, indicating a 0.1 mm radius difference between the 5th and 6th orders, with subsequent orders maintaining <0.1 mm differences. When replacing the linear requirement with 0.05 mm, the solution becomes $l_{\text{lim}} = 24$, meaning any adjacent topological charge within order 25 maintain a vortex beam radius difference greater than 0.05 mm. These calculations are based on the $z = 0$ source plane. For more general cases, simply replace w_0 with w_z.

3.4. Absorption ratio of Gaussian vortex beam

One of the most distinctive features of vortex light is its central "black spot" that emits no light. This region, where the central area has zero light intensity and lacks energy distribution, creates a physical "vacuum" state. Furthermore, vortex beams with $l > 0$ can be combined with other light sources for information encryption transmission. For vortex light with a topological charge of l, the area of the luminous region can be determined by measuring the inner and outer ring radii. According to Eq. (16), the extinction ratio represents the proportion of the non-luminous region relative to the total area. Below we calculate the extinction ratio of a Gaussian vortex light.

Assuming that the topological charge is l, the inner radius of the vortex beam is r, the outer radius is R, and the ring thickness is d, the extinction ratio expression can be obtained from (13) and (16):

$$\Lambda = \frac{2(R-d)^2}{(2|l|+1)\omega_z^2} \times 100\% \tag{19}$$

Based on Eq. (19), after determining the propagation distance z and vortex halo thickness d, the relationship between extinction ratio and propagation distance z and l can be obtained as:

$$\Lambda = \frac{2B(R-d)^2}{(2|l|+1)(z+Z_R)^2} \times 100\% \tag{20}$$

Among them $B = (Z_R/w_0)^2$, because the actual laser has different structural differences and it is difficult to obtain the beam waist radius w_0 and other related parameters, the simplified extinction ratio approximation expression is:

$$\Lambda = \left[1 - \frac{2d}{R} + \left(\frac{d}{R}\right)^2\right] \times 100\% \tag{21}$$

As shown in Eq. (21), as the radius R between adjacent topological flux vortex beams decreases, the thickness d of the vortex halo also diminishes. When d approaches the linear dimension of R (R ranges from 10 to 100), the magnitude of d becomes extremely small, causing the extinction ratio to approach 1. Since R is included in the denominator (which contains propagation distance z), when we exclude the source plane $z = 0$, the extinction ratio will converge to 1 more rapidly.

4. Experiments and results

The imaging effect of Gaussian vortex light is achieved by constructing the optical path as shown in Fig. 8. The equipment used includes: a 532 nm Gaussian laser, an expander, a polarizer, a reflective pure-phase modulated LCoS, a custom beam-splitting cube with integrated mirrors. The difference in wavelength between the experimental light source and the simulated light source is due to the fact that the 532 nm laser used in the laboratory belongs to the visible light range, making it more convenient for direct observation compared to the near-infrared 867.7 nm wavelength. The laser first undergoes expansion and collimation through the expander, then becomes horizontally polarized via the polarizer. It subsequently passes through the preloaded grating vortex -phase LCoS, and finally forms an image on the imaging screen via the lens. The CCD captures interference patterns with 10 different topological charges as shown in Fig. 9. This demonstrates that the imaging interference pattern of vortex light indeed differs from conventional Gaussian interference patterns.

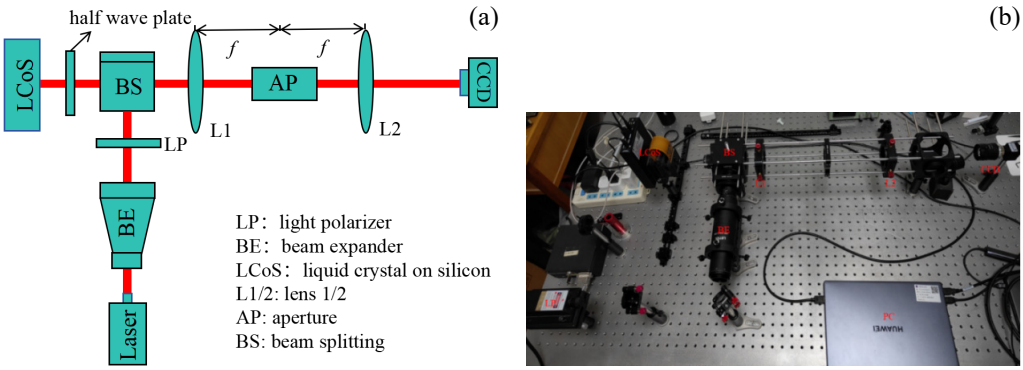

Fig. 8. Schematic diagram of vortex beam imaging experiment (a) and experimental device (b).

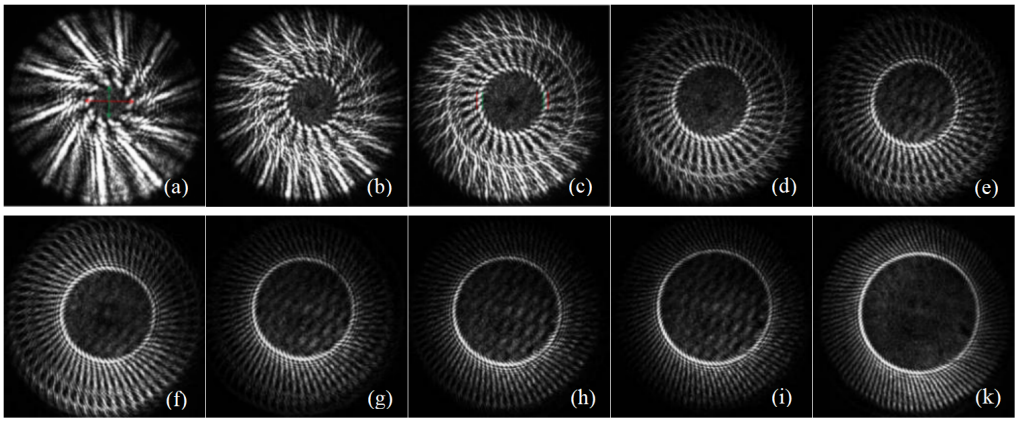

Fig. 9. Hollow vortex light generated by different topological charges (l = 10, 20, …, 100) on CCD.

After directly reading the vortex imaging on the CCD detector, we used a drawing tool to identify pixels at the tangential positions of inner and outer diameters to determine the "hollow" inner and outer ring diameters r and R. These correspond to the measurement methods shown by the green and red lines at l = 10 in Fig. 9(a). Based on Eq. (21), the extinction ratios of these 10 vortex patterns are summarized in Table 2, with their variations with topological charge shown in Fig. 10. The analysis yields the following conclusions:

1) All 10 images exhibit hollow vortex extinction phenomena in the central region, where the hollow dark spots increase with increasing topological charge;

2) Beyond the hollow structures, multi-level alternating circular interference fringes appear, with the number of interference phases matching the topological charge. As the topological charge increases, the central pattern that should be circular increasingly resembles simulated images;

T a b l e 2. Extinction ratio of different topological charges directly measured on CCD (unit: pixel).

l	External conjugate $2R$	Internal conjugate $2r$	Thickness d	Light extinction percentage
10	105	70	17.5	44.44%
20	135	109	13	65.19%
30	160	136	12	72.25%
40	180	160	10	79.01%
50	198	180	9	82.64%
60	217	197	10	82.42%
70	231	212	9.5	84.23%
80	246	229	8.5	86.66%
90	260	242	9	86.63%
100	272	254	9	87.20%

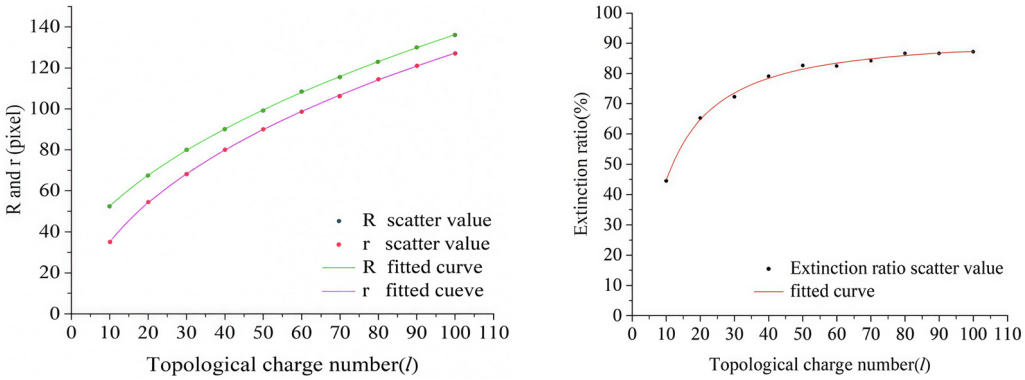

Fig. 10. Variation inner and outer ring radii (a) and extinction ratio (b) with topological charge.

3) The number of outward radiating interference fringes corresponds to the topological charge;

4) Although extinction ratios gradually increase with topological charge, faint alternating bright-dark fringes emerge within the hollow regions;

5) The experimental results in Fig. 10 show a similar trend to the theoretical simulations in Figs. 5 and 7.

5. Conclusions

This study investigates the extinction characteristics of hollow regions in Gaussian vortex light. By simulating vortex beams with topological charges of 0, 1, and 2, we observed distinct "hollow" extinction phenomena. We then derived the relationship between vortex beam radius and topological charge, formulated expressions for hollow extinction ratio and vortex beam radii. The results revealed a linear correlation between extinction ratios and topological charges (from 1 to 20). The fitted error rate between theoretically calculated hollow radii and simulated radii reached 85.93%, with an average deviation of 17%. Using a laser system fabricated with LCoS technology, we generated 10 interference fringes of hollow vortex light with topological charges ranging from 10 to 100 using a 532.0 nm wavelength laser on a CCD detector. Pixel measurements of inner and outer radii corresponding to these topological charge patterns were conducted, enabling precise calculation of extinction ratios. Experimental data confirmed the theoretical predictions through linear variations in hollow radii with topological charges.

Acknowledgment

This work was supported by Scientific Research Program Funded by Natural Science Basic Research Program of Shaanxi (Grant No. 2025JC-YBMS-059) and Shaanxi Provincial Education Department (Grant No. 23JP118, Grant No. 24JP114)

Reference

[1] Eyyuboğlu H.T., *Mutual coherence function based topological charge detection in a Gaussian vortex beam optical communication system*, Physica Scripta **97**(9), 2022: 095507. https://doi.org/10.1088/1402-4896/ac8956

[2] Otte E., Denz C., *Optical trapping gets structure: Structured light for advanced optical manipulation*, Applied Physics Reviews **7**(4), 2020: 041308. https://doi.org/10.1063/5.0013276

[3] Lin Z.Z., Hu J.Q. Chen Y.J., Yu S.Y., Brès C.S., *Spectral self-imaging of optical orbital angular momentum modes*, APL Photonics **6**(11), 2021: 111302. https://doi.org/10.1063/5.0067668

[4] Li Y.S., Chen J., Fu G.K., Qi G.Z., Shi Y., Zhao C.L., Jin S.Z., *Measurement of topological charge of obstructed wandering vortex beams*, Acta Optica Sinica **43**(2), 2023: 0226002 (in Chinese). https://doi.org/10.3788/AOS0226002

[5] Chen G.M., Lin H.C., Pu J.X., *Generation of high-order Bessel beams by focusing vortex beams with an axicon*, Guangdianzi Jiguang/Journal of Optoelectronics Laser **22**(6), 2011: 945-950 (in Chinese).

[6] Oemrawsingh S.S.R., Ma X., Voigt D., Aiello A., Eliel E.R., 't Hooft G.W., Woerdman J.P., *Experimental demonstration of fractional orbital angular momentum entanglement of two photons*, Physical Review Letters **95**(24), 2005: 240501. https://doi.org/10.1103/PhysRevLett.95.240501

[7] Heckenberg N.R., McDuff R., Smith C.P., White A.G., *Generation of optical phase singularities by computer-generated holograms*, Optics Letters **17**(3), 1992: 221-223. https://doi.org/10.1364/OL.17.000221

[8] Ma H.T., Zhou P., Wang X.L., Ma Y.X., Wang X.B., Xu X.J., Liu Z.J., *Coherent beam combining of fiber amplifiers based on stimulated annealing algorithm*, High Power Lasers and Particle Beams **22**(5), 2010: 973-977.

[9] Karimi E., Schulz S.A., De Leon I., Qassim H., Upham J., Boyd R.W., *Generating optical orbital angular momentum at visible wavelengths using a plasmonic metasurface*, Light: Science & Applications **3**, 2014: e167. https://doi.org/10.1038/lsa.2014.48

[10] Coullet P., Gil L., Rocca F., *Optical vortices*, Optics Communications **73**(5), 1989: 403-408. https://doi.org/10.1016/0030-4018(89)90180-6

[11] Curtis J.E., Koss B.A., Grier D.G., *Dynamic holographic optical tweezers*, Optics Communications **207**(1-6), 2002: 169-175.

[12] Bo B., Menke N., Zhao J.L., Cheng M., Du J., Ning A.Q., *Generation of vortex beams with a reflected type phase only LCSLM*, Guangdianzi Jiguang/Journal of Optoelectronics Laser **23**(1), 2012: 74-78 (in Chinese).

[13] Zhang H., Yuan Y.S., Cai Y.J., *Research on vortex beams applied in optical communications*, Journal of Shandong Normal University (Natural Science Edition) **39**(2), 2024: 97-116.

[14] Liu Y.H., Tang Y.H., Zhou J., Li C.X., Hui N.J., Zhang Y.S., Wang Y.L., *Study on the imaging interference of a vortex-light-modulated Gaussian beam*, Photonics **11**(6), 2024: 557. https://doi.org/10.3390/photonics11060557

[15] Yin Z.Q., Wu C., Gong W.Y., Gong Z.K., Wang Y.J., *Voigt profile function and its maximum*, Acta Physica Sinica **62**(12), 2013: 123301 (in Chinese). https://doi.org/10.7498/aps.62.123301

[16] Curtis J.E., Grier D.G., *Structure of optical vortices*, Physical Review Letters **90**(13), 2003: 133901. https://doi.org/10.1103/PhysRevLett.90.133901

[17] Scott A., Zheng S.H., Brown S., Bell A., *Spatial heterodyne spectrometer for FLEX*, Proceedings of the SPIE, Vol. 6744, Sensors, Systems, and Next-Generation Satellites XI, 2007: 67441W. https://doi.org/10.1117/12.737083

Received August 18, 2025
in revised form September 29, 2025